Journal of Fluid Science and Technology

Vol. 2, No. 2, 2007

Three-Dimensional Micro Propeller Design by Using Efficient Two Step Optimization*

Ki-Hak LEE**, Yong-Hee JEON**, Kyu-Hong KIM**, Dong-Ho LEE** and Kyung-Tae LEE***

**School of Mechanical and Aerospace Engineering, Institute of Advanced Aerospace Technology, Seoul National University

San56-1 Shinlim-dong, Kwanak-ku, Seoul, Republic of Korea

E-mail: donghlee@snu.ac.kr

*** School of Mechanical and Aerospace Engineering, Sejong University

98 Gunja-dong, Kwangjin-ku, Seoul, Republic of Korea

Abstract

A practical and efficient optimal design procedure is presented for three-dimensional micro-propeller. To manage many design related variables and operating conditions efficiently, the design procedure consists of two steps for optimization of operating conditions and blade geometries. First, operating condition points are extracted from the design-of-experiments, and provided as the input data of the geometry optimization step. Next, in the geometry optimization step, the 2-D airfoil shapes are optimized to provide the maximum lift-to-drag ratio along the radial blade section by using the XFOIL code, and the 3-D blade shapes are determined at the each operating condition by using the minimum energy loss method. Then, the performances of the optimized blade are calculated, and a Response Surface Model is constructed to decide the operating condition for the maximum propeller efficiency. To find the blade shape with better performance than the optimum shape in the initial design space, the design space is modified to a highly feasible design space by using the probability approach. Finally, the performance of the optimized propeller is compared with that of the Black Widow MAV propeller. The comparison showed that the optimized propeller had somewhat better performance. The present optimal design procedure is reliable and can be used as a practical design tool for micro propeller development.

Key words: Propeller, Micro-Air Vehicles, XFOIL, Design Optimization, Response Surface Method, Probability Approach, Minimum Energy Loss

1. Introduction

Recently, Micro-Air Vehicles (MAVs) have been designed not only for special, limited-duration military applications, but also for commercial applications.(1) Although MAVs may be used in the very near future, more investigations are still necessary on the low Reynolds number (*Re*) aerodynamics, efficient electronic motors and optimized propellers. The comparison of the total mass ratio of a propulsion system to a vehicle showed that the mass ratio of a fixed-wing MAV was larger than that of a conventional aircraft. Thus, the efficiency of MAVs propulsion system is an important issue. One of the most effective ways to improve the efficiency of a propulsion system is to design an optimum propeller because the propeller performance is a crucial factor for the success of fixed-wing MAVs(2).

There are two kinds of design methods that are applied to the design of micro

*Received 27 Feb., 2007 (No. 07-0104)
[DOI: 10.1299/jfst.2.334]

propellers. The first one is the direct numerical optimization method, which can consume a great amount of time to converge results by iteration of the design process. In addition, nonlinear problems with many design variables by Computational Fluid Dynamics (CFD) analysis of entire 3-D flow fields is practically getting more difficult because of tremendous time for analysis and intensive computing power needed to iterate the design process[3]. Compared with the direct numerical optimization method, the inverse design method has an advantage of convergence in less time by iteration of the design process.

To solve such problems in this study, Glauert's strip theory[4], which is a combination of the momentum theory and the blade element theory is adopted. The applied inverse method has been developed which is based on the propeller design theory of Prandtl and Betz[5] for the minimum energy loss conditions. Larrabee[6] resurrected the propeller design equations and presented a straightforward procedure for optimum propeller design. Adkins and Liebeck[7] improved the design of optimal propellers without the assumptions of any small angle and light-load. However, these inverse design methods also have limitations in blade geometry design, and do not explain in detail the optimum propeller design procedure with respect to the operating condition parameters and various constraints. *Therefore, for the development of a more enhanced propulsion system, it is necessary to study a reasonable and efficient propeller design optimization process by combination of the inverse design and the direct numerical optimization method including these operating condition parameters and various constraints*. Lee et al.[8] as the previous study presented the design optimization procedure for the micro propeller.

The aim of the study is to maximize the efficiency of the micro-sized propellers for MAVs and to develop a reliable design procedure that can quickly optimize both the geometry and operating condition. The performance of the optimized propeller in this design procedure is validated by comparing with that of Black Widow MAV[2].

2. Efficient Design Strategy for Micro Propeller: Two Step Optimization

2.1 Design Objective

The nominal mission profile for the fixed-wing MAVs is to climb to about 60-200 m above the ground level, and to cruise around at the optimum loiter velocity to gather video data. Since the MAVs spend more than 90% of their flights at the loiter flight condition, the propeller optimization is greatly simplified[2]. The objective function is to maximize the endurance of the MAVs, which has a one-to-one correspondence with the minimization of the required total power, P_{total}. P_{total} for operating MAVs is derived by Eq. (1).

$$P_{total} = \frac{W}{\eta_p}\left(\frac{W}{S}\right)^{\frac{1}{2}}\left(\frac{2}{\rho}\right)^{\frac{1}{2}}\left(\frac{C_{D,wing}}{C_{L,wing}^{3/2}}\right) \tag{1}$$

In this equation, S is the wing area, and ρ is the air density which involves the altitude of a mission profile. Since the weights of electrically powered vehicles, W, the vehicle's wing shape, the lift coefficient of the wing, $C_{L,wing}$, the Drag coefficient of the wing, $C_{D,wing}$, and ρ are all fixed to the same values, respectively, the propeller efficiency, η_p, is directly affected by P_{total}, as shown in Eq. (1), and should be maximized. That is, our objective function, the maximization of the endurance of the MAVs equals the maximization of η_p.

2.2 Design Constraints

The first constraint considered in this study is the required thrust, T, that is set to the drag at the loiter velocity because MAVs propeller is designed at the loiter velocity. T was set as 9.9 g_f, which was the same as the drag of Black Widow MAV for the geared propeller configuration at the loiter velocity, V_∞, of 11.176 *m/s*. [2] An additional positive 3% T is allowed in the equality constraint of T.

$$T = 9.9 g_f = 0.09709 N \quad (\leq +3\%) \tag{2}$$

The second constraint is the activity factor (AF), which is a measure of the effect of blade width and the distribution of the chord length, c, on the propeller. The value of a blade AF is a non-dimensional number, and represents the solidity or geometrical shape of the blade. AF of a practical propeller ranges from about 90-200 in Eq. (3) [9].

$$90 \le AF \le 200 \tag{3}$$

$$\text{where,} \quad AF = \frac{10^5}{D^5}\int_{hub}^{tip} cr^3 dr = \frac{10^5}{D^5}\int_{0.15R}^{1.0R} cr^3 dr$$

Here, R is the propeller blade radius, D is the blade diameter, and r is the blade radial coordinates. Because the blade roots are usually shielded by a spinner, the limit of the integral for AF changes from zero (the root) to $0.15R$.[10]

To obtain a higher propeller performance, a larger propeller has to be used because it can distribute its power into propeller, P, and T on a larger incoming fluid volume. However, for low noise and compressibility effect, the upper limit of the Mach number at the blade tip, M_{tip} should be about 0.63.[9] Thus, M_{tip} as the third constraint for the upper limit then follows from Eq. (4).

$$M_{tip} \le 0.63 \tag{4}$$

$$\text{where,} \quad M_{tip} = \sqrt{M^2 + \left(\frac{\pi n D}{a}\right)^2}$$

Here, M is the Mach number, a is the speed of sound, and n is the propeller revolution per second (rps).

2.3 Two Step Optimization and Design Variables for Each Step

As the number of design variables increase in 3-D propeller design, the required design points increase by geometric progression, and tremendous time and computing power are needed to iterate the process. The design variables in each step are shown in Table 1.

Table 1 Design variables and methodologies applied to each design step.

Design steps		Design variables (DV)	# of DV
Step 1. Operating condition optimization		x_1 : power into propeller (P) x_2 : propeller rpm x_3 : blade diameter (D)	3
Step 2. Geometric shape optimization	Blade shape design	x_4 ($x_{4\text{-}1}$-$x_{4\text{-}10}$)* : chord length (c)	10
		x_5 ($x_{5\text{-}1}$-$x_{5\text{-}10}$) : pitch angle (β)	10
	Airfoil shape design	x_6 ($x_{6\text{-}1}$-$x_{6\text{-}120}$) : 12 weighting coefficients at each airfoil	120

* *10 blade radial sections*

The propeller design process with overall 143 design variables simultaneously is next to impossible at present. To manage efficiently many designs, the design procedure involves an operating condition optimizer and a blade geometry optimizer. The design variables x_1-x_3 for the operating condition optimization are P, rotating speed (revolution per minute, rpm), and D. The design variables x_4 and x_5 for the blade shape design are the geometries of propeller including the blade pitch angle, β, and c at each radial blade section. The design variables x_6 for the airfoil shape design include 12 weighting coefficients on each airfoil surface. To reduce the complexity of the system, the propeller is assumed to be a fixed pitch propeller. The number of blades is set to 2 because it has a small effect on the efficiency of the propeller and reduces the propeller complexity, cost, and weight.[10]

With respect to the range of design variables, the design space must be carefully chosen to satisfy the design requirement and purpose, especially in the initial design phase. In this

study, based on the propeller performance data of the Black Widow MAV[2], the initial design ranges of η_p and J are set. The following Eq. (5) shows the details.

$$0.70 \le \eta_p = \frac{TV_\infty}{P} \le 0.90 \qquad D = \frac{0.80}{0.95} \times 0.6 \times \sqrt[4]{P\,[kW]} \qquad 1.00 \le J = \frac{60 \cdot V_\infty}{rpm \cdot D} \le 1.55$$

$$\Rightarrow \quad 1.21 \le P = \frac{TV_\infty}{\eta_p} \le 1.55 \;\; [W] \qquad 0.09415 \le D \le 0.10025 \;\; [m] \qquad 4315 \le rpm = \frac{60 \cdot V_\infty}{J \cdot D} \le 7122 \tag{5}$$

The overall design optimization process to improve the efficiency of propeller is shown in Fig. 1. In the operating condition optimization step (Step 1), the design space is composed of the design variables x_1-x_3. Operating condition points extracted from the design-of-experiments (DOE)[11] are provided as the input data of the geometry optimization step (Step 2). Next, in Step 2, the 2-D airfoil shapes are optimized to provide the maximum lift-to-drag ratio, L/D_{max}, along the radial blade section by using the XFOIL code[12] and the Hicks-Henne shape functions[13], and the blade shapes are determined by using the strip theory for the minimum energy loss condition[7] at each operating condition. Then, the performances of the optimized blade shape are calculated, and return to Step 1. For the efficiency of the design procedure, the Response Surface Methodology (RSM)[11] based on the calculated performances in Step 2 is adopted. x_1-x_3 are optimized as the values at the operating condition with the maximum propeller efficiency under several constraints such as T, AF, and M_{tip}.

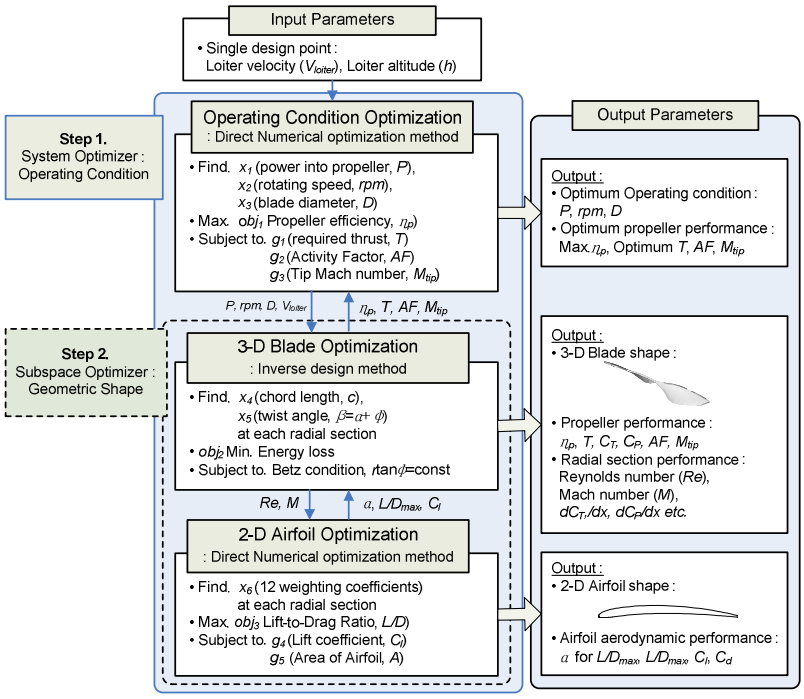

Fig. 1 Two step design optimization process for 3-D propeller blade.

3. Design Methodologies of Each Step

3.1 Step 1: Operating Condition Optimization

To find the maximum η_p and the optimum design variables of the operating condition, the design process requires many data points and much analysis time. To reduce the calculation time for the analysis, one of the representative approximation methods, RSM, is used with operating condition data points. To build the RS model, 3^k full factorial DOE and

second order full regression model are utilized, and then, the confidence level of the RS model is checked by the analysis of variance.[11] The RS model usually assumes a simple second order polynomial mathematical model. For the RS model with 3 design variables, the number of data points is 27.

For a reliable design via the RS models, the error should be small. The typical values of R^2_{adj}, which is the measure of reliability associated with organized RS models, range from 0.9 to 1.0, and the closer this value is to 1, the more accurately RS model is constructed.

The operating condition optimization is performed by applying the objective and constraints with the constructed RS models. The Sequential Quadratic Programming (SQP) method[14], which is one of the direct numerical optimization methods, is used for design optimization.

3.2 Step 2: Geometric Shape Optimization

Propeller Blade Shape Optimization

The design procedure includes the blade geometry design in terms of both the chord distribution and the blade twist angle distribution. In this study, the strip theory given by Adkins and Liebeck[7] is adopted as the inverse design method of optimum propellers. The strip theory, which combines the momentum theory and blade element theory, satisfies the Betz condition for minimum energy loss. To do this, the angle of attack, α, corresponding to L/D_{max} should be specified at each section. It establishes the iterative design and analysis procedures, which can determine the geometry and performance of a propeller quickly. And, it iterates to find β and c distributions, radial and axial interference factors, Re, and relative M depending on the operating condition. The details are described in Ref. 7.

Airfoil shape optimization

To enhance the efficiency of the propeller, the airfoil shape is optimized such that the lift-to-drag ratio, L/D, is maximized at each blade section airfoil. To analyze the aerodynamic performances of the airfoil, the XFOIL code[12] is used. XFOIL code is a tool for both inviscid and coupled inviscid and boundary-layer flows around airfoils in steady, subsonic flow. It uses the e^n method, which is a two-equation boundary layer integral formulation based on the dissipation closure for both laminar and turbulent flows. The overall design procedure for a propeller usually demands many iteration numbers. With respect to this demand, the XFOIL code is far better than other codes, such as the Navier-Stokes code, and yields acceptable accuracy in low Re flow analysis.

The form of the airfoil optimization problem can be stated as:

$$\textit{Maximize} \qquad L/D = C_l / C_d \tag{6}$$

$$\textit{Subject to} \qquad \begin{aligned} C_l &\geq C_{l_0} \\ A &\geq 0.5 \times A_0 \end{aligned} \tag{7}$$

where, L/D, C_l, C_d, and A are the lift-to-drag ratio, the lift coefficient, the drag coefficient, and the cross section area of designed airfoil, respectively. The subscript *0* stands for the initial values of an initial airfoil. While L/D_{max} of an airfoil for a low-speed conventional aircraft with a fixed wing is greater than 10, L/D_{max} of an airfoil for the MAVs propeller is usually less than 10 in the low Re flow regime. To enhance L/D at low Re, an optimized airfoil must be very thin (i.e., t/c < 0.06) with a modest amount of camber.[15] Thus, an airfoil area is allowed to be over half of the initial value. Since most of micro propellers are solid type, it does not matter structurally even though airfoil will be very thin.

The airfoil shape is modified by adding a smooth perturbation to the initial airfoil. In this study, a set of Hicks-Henne shape functions[13] are adopted. The each airfoil geometry is modified with 12 shape functions (i.e., 12 design variables), six each in the upper and lower surfaces of the airfoil.

4. Improvement of the Design Space Feasibility

Generally, designers have selected a design space that is reasonable through their intuition or empiricism. However, this initial design space may be mixed with *the feasible region which satisfies all constraints*[16] and the infeasible region. Although an optimum point would be found in the given initial design space, one can argue that it is not the global optimum and the better optimum point may appear outside of the initial design space. To find a global optimum, an exploration of the design space requires that the feasibility of the design space is improved and that the infeasible region is removed.

In this study, the probability approach is employed to improve the available feasible design space.[17] For this approach, we first construct the RS models with respect to the constraints of the operating condition optimization. Then, to find the feasible region, Monte Carlo Simulation (MCS) in which one million random sample points are generated with uniform distribution and the standard normal distribution is adopted. The mean, μ, and the standard deviations, σ, of the design variables can be calculated by using MCS. The probability of success is the probability which satisfies all constraints. As the probability of success increases, the feasible region becomes larger. The details are described in Ref. 17.

The ranges of the design variables are modified by using Chebyshev's inequality condition to improve the feasibility of design space. Chebyshev's inequality condition can be written as:

$$P(\mu - k\sigma \le x \le \mu + k\sigma) \ge 1 - \frac{1}{k^2} \tag{8}$$

Regardless of the actual distribution of the random sample points, if k equals 3, any design variable has a probability of at least 89 % of taking a value within 3σ of its μ. The range of the design variables, x_1-x_3 is re-adjusted from μ -3 σ to μ +3 σ in Eq. (8). In this study, this process is repeated until the variance of the probability of success converges within the convergence criteria (1 %) based on the value in the previous step[18].

5. Results and Discussions

The flowchart of each design case is represented in Fig. 2. In Case 1, the design optimization with ARA-D 6% airfoil is performed. That is, because the 2-D airfoil design is excluded, only 23 design variables of x_1-x_5 in table 1 are used. Case 2 includes the 2-D airfoil shape design additionally based on Case 1; the design variables are increased up to 143 including 120 design variables for the airfoil shape design. To find a global optimum outside of the initial design space, the design optimization by using the probability approach in Case 3 is performed based on the results of Case 2.

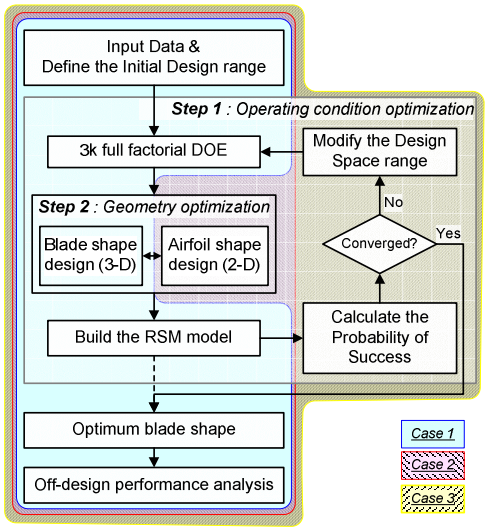

Fig. 2 Flowchart of Case 1, Case 2, and Case 3.

5.1 Case 1: Design Optimization Excluding the Airfoil Design

Before the optimization procedure for our application process, it is necessary to verify the computational accuracy of XFOIL to predict the 2-D airfoil performance. However, an airfoil of the micro-propeller is very small and operate at the low Re below 30,000 where very little experimental data available. In Fig. 3, the calculated lift and drag of Eppler 61 airfoil at Re of 25,000 is compared to the available experimental data[19]. The turbulence intensity up to about 1 % does not have a strong effect on the lift and drag of thin airfoils at low Re. Thus, the e^9 method, with the critical disturbance parameter, n_{crit}, is set to 9, which

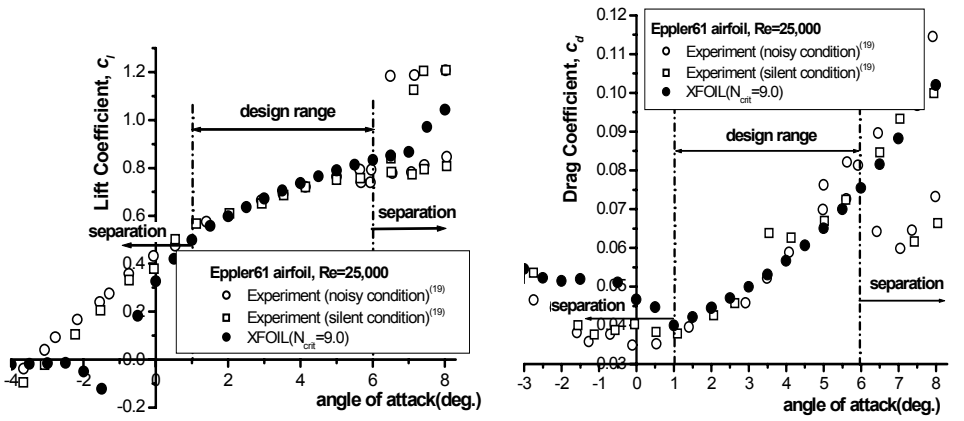

(a) Lift coefficient (C_l) (b) Drag coefficient (C_d)

Fig. 3 Comparison of the predicted C_l and C_d of 2-D Eppler61 airfoil by XFOIL, Re=2.5 x 10^4.

corresponds to the turbulence level of 0.07 % and is used as the most common choice. The results of XFOIL correspond with the experimental results except for the largely separated region, below α=1° or over α=6°. Outside this range, XFOIL cannot predict the aerodynamic features accurately owing to the separation.

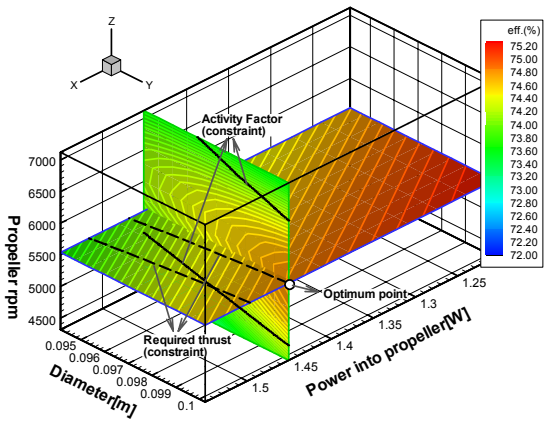

Fig. 4 Objective function and constraints contour in the design space for Case 1.

In this study, ARA-D 6% airfoil on the entire span is chosen as the initial airfoil for the propeller blade design because the aerodynamic performance of the ARA-D 6% airfoil is greater than those of other airfoils.[8]. ARA-D 6% airfoil, which has 6.02 % thickness-to-chord ratio and 5.01 % camber-to-chord ratio, is a relatively thinner and larger cambered than other various propeller section airfoils.

Next, we perform the design optimization with the ARA-D 6% airfoil on the entire space. As shown in Fig. 4, the optimum values of the design variables are 1.451 W for power, 0.1003 m for diameter, and 5535 for rpm in the design space and the maximum η_p reaches 74.8 %. This optimum point stands on the maximum diameter in the design space of x_1-x_3.

5.2 Case 2: Design Optimization Including the Airfoil Design

First, we checked whether or not the α range with L/D_{max} was between 1-6° where XFOIL is validated. Figure 5 shows the comparison of L/D distributions with respect to Re and α within the design range. L/D of the optimized airfoils seems to be enhanced by 38 % in comparison with that of the ARA-D 6% airfoil.

The optimized airfoils along the radial section have somewhat similar shapes. The optimized airfoil shape at the 78 % section along the radius is shown in Fig. 6. The optimized airfoil has 4.55 % maximum thickness at the 0.088x/c and 4.51 % maximum camber at the 0.493 x/c. In comparison to the values of maximum thickness and camber of the ARA-D 6% airfoil, those values of the optimized airfoils are reduced by 32.3 % and 11.1 %, respectively. Since the leading edge curvature remains blunt, it can prevent the occurrence of a leading edge stall. The flat upper surface of the optimized airfoil throws back the flow separation, and the aerodynamic performances are strongly enhanced within the α range between 1-6°.

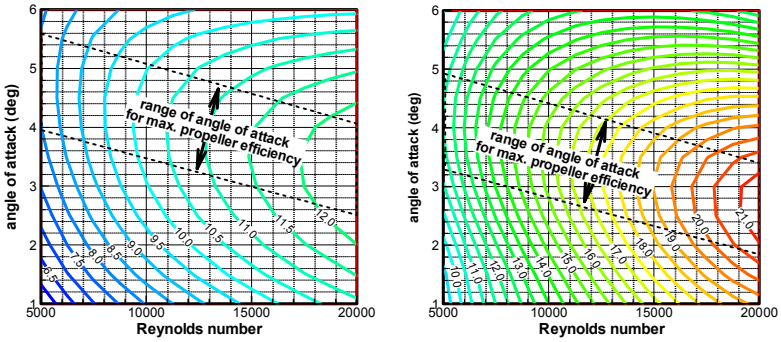

(a) *L/D* distribution of ARA-D 6% airfoil (b) *L/D* distribution of optimized airfoils

Fig. 5 Comparison of *L/D* distributions.

Figure 7 shows that throughout the optimization process, that the optimum values of the design variables are 1.341 *W* for *P*, 0.1003 *m* for *D*, and 5802 for rpm in design space, and the maximum η_p reaches 80.9 %, which is an increase of 6.1 % over that of Case 1. Like Case 1, this optimum point also stands on the maximum *D* in the design space of x_1-x_3.

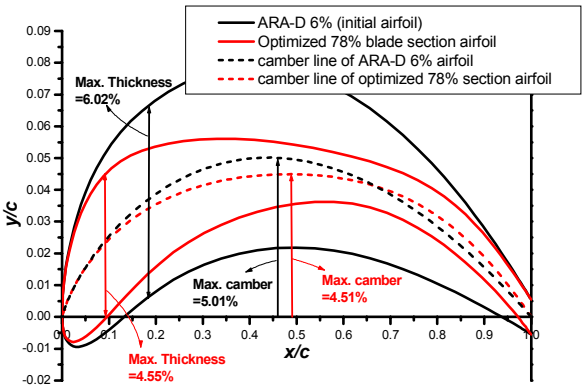

Fig. 6 Comparison of the optimized airfoil shape with ARA-D 6% airfoil shape.

5.3 Case 3: Design Optimization by Adding the Probability Approach

In Cases 1 and 2, the optimum points stand on the maximum *D*, i.e., it is much probable that there is the better optimum position outside the initial design space of x-x_3. Thus, the design space should be modified into an improved design space by using the probability approach. Thus, the design optimization by using probability approach in Case 3 is performed based on the results of Case 2.

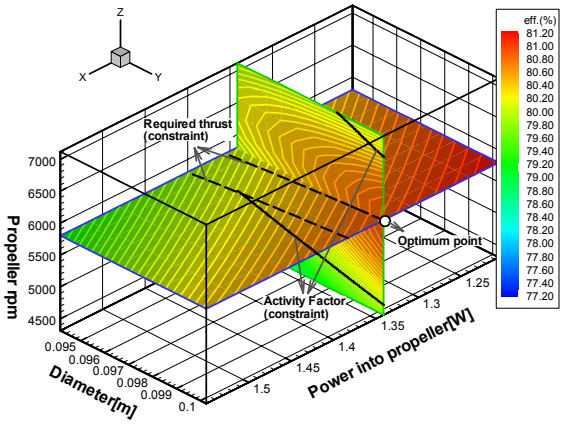

Fig. 7 Objective function and constraints contour in the design space for Case 2.

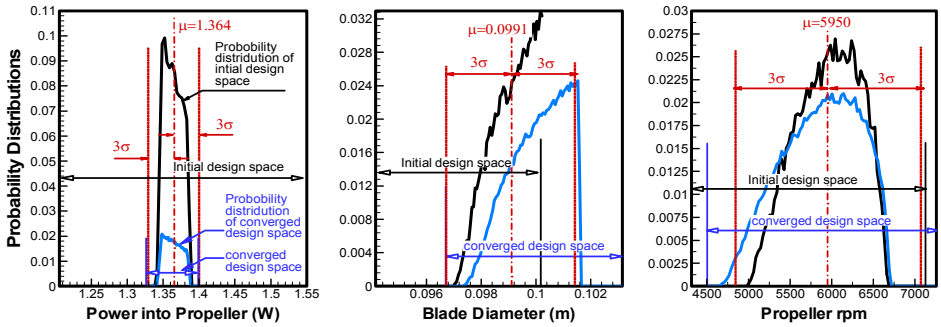

Fig. 8 Probability distribution of the design variables in the operating condition.

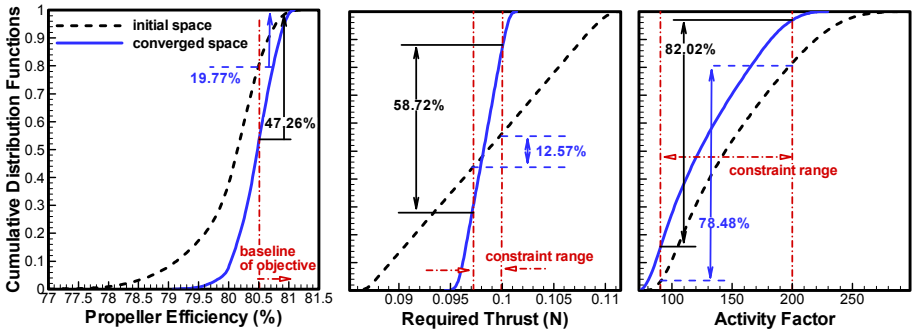

Fig. 9 Joint CDF of the design performance of Case 3 design results.

MCS employing uniform distributions of the operating condition design variables is performed to generate one million sample points for the objective and constraints. At this Case, the baseline value of the objective function as η_p is set 80.5 %. Since only 22,213 points among the one million data points belong to the feasible region, the probability of success for the initial design space is 2.22 %. The probability distributions of the design variables are represented in Fig. 8. The initial design space yields μ of 1.364 *W* with σ of 0.0119 *W* for *P*, μ of 0.0991 *m* with σ of 0.000767 *m* for *D*, and μ of 5950 with σ of 374.5 for rpm. The probability distribution of the success range for *P* is a narrow range, and the range for *D* inclines to the maximum in the initial design space. In converged design space, the *P* range is reduced and the *D* range increases to the right by using Chebyshev's inequality condition.

To investigate the probability of success of satisfying the objective and constraints, joint CDF are represented in Fig. 9. Since M_{tip} satisfies the constraint condition in the initial and converged design spaces, its constraint has no effect on the modified design space. By modifying the design space, the probability of success becomes 47.26 % for η_p, 58.72 % for *T*, and 82.02 % for *AF*. Moreover, the total probability of success in the converged space reaches to 16.67 %. Thus, η_p can produce better optimized solutions in the converged design space than in the initial space.

Figure 10 represents the comparison of the initial and converged design spaces for η_p and constraints in the Case 3 design. Compared with the design ranges for *P*, *D*, and rpm in the initial design space, the ranges of *P* and rpm of the converged space are reduced and the range of *D* moves beyond the upper bound of the initial space. As a result, the global optimal point is located at the new space outside the initial design space. In the converged design space, the global optimum point is 1.340 *W* for *P*, 0.1016 *m* for *D*, and 5666 for rpm, respectively. Owing to the constraint related with *T*, the value of D has the upper limit. The η_p is maximized up to the value of 81.0 %.

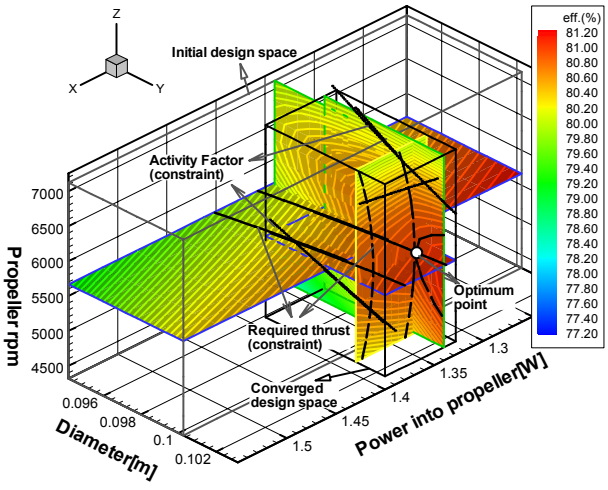

Fig. 10 Objective function and constraints contour in the initial and converged design space.

5.4 Comparison of Results for Each Case

R^2_{adj} calculated to confirm the reliability of the RS models for Cases 1, 2, and 3 are

Table 2 Design parameter results for optimum propeller configurations.

Operating condition design parameters		Case 1	Case 2	Case 3	Black Widow MAV[2]
Design variables	Power into propeller, *P (W)*	1.451	1.341	1.340	1.356
	Blade diameter, *D (m)*	0.1003	0.1003	0.1016	0.0968
	Propeller rpm	5535	5802	5666	5365
Objective	Propeller efficiency, η_p *(%)*	74.8	80.9	81.0	80
constraints	Activity Factor, *AF*	131.6	121.0	122.2	Unknown
	Required thrust, *T (N)*	0.0971	0.0971	0.0971	0.0971
	Tip Mach number, M_{tip}	0.0912	0.0952	0.0943	0.0906
Type of section airfoil on the entire span		ARA-D 6%	Optimized	Optimized	Unknown
Number of blade section		10	10	10	Unknown

more than 0.99, which guarantees the reliable construction of the RS models.

In Table 2, all the optimum values of the design parameter are compared with each case. Owing to the airfoil design in Case 2, *P* is decreased by 8.2 % and η_p is increase by 6.1 %, compared with Case 1. The maximum η_p of Case 3 do not greatly increase in comparison with that of Case 2 because the reasonable initial design space of Case 2 is set up based on the data of Black Widow. However, improvement of the feasibility of the design space in Case 3 guaranteed that the better optimum could find in a new design space. In case that such a high level of information is not available any more, the present probability approach study may be useful. The reliability of the design process is validated by comparison with the design parameters of the Black Widow MAV. Although the optimum blade of Case 3 is slightly longer and faster than that of Black Widow MAV, the optimum *P* of Case 3 is 1.20 % less and the maximum η_p is 1.0 % higher.

Figure 11 shows the performance distributions of the optimized micro-propeller blades with respect to the radial direction. Compared to Case 1, because of the increase of the rpm of Cases 2 and 3 with the decrease of *P* in Table 2, *c* distribution is reduced in Fig. 11 (a);

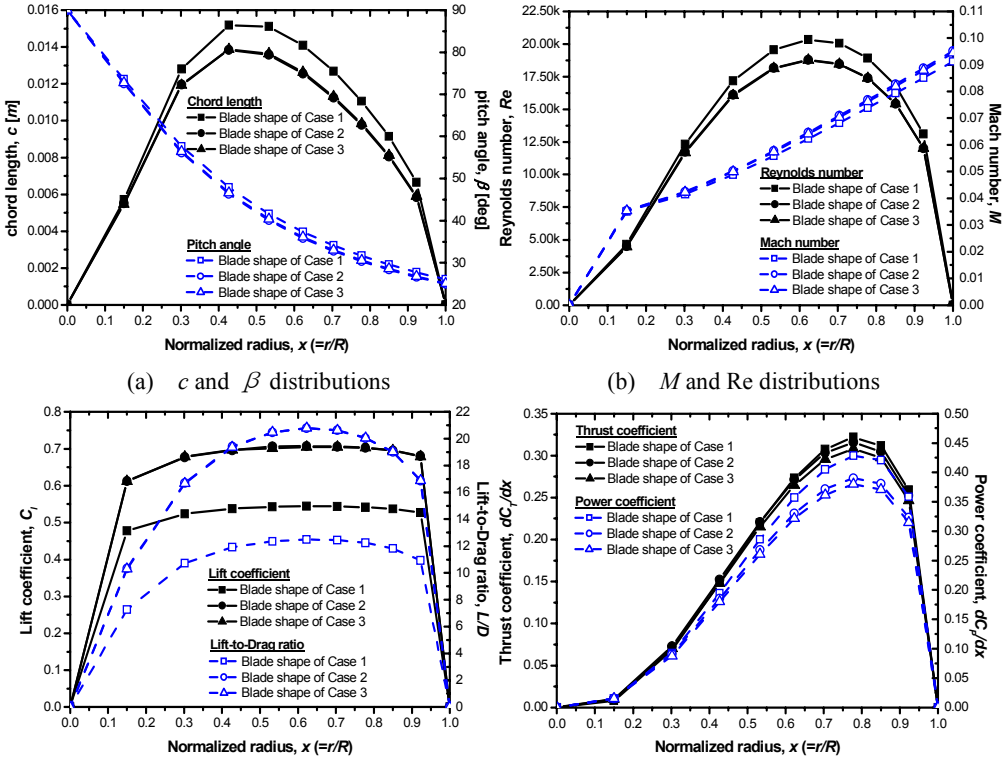

(a) c and β distributions

(b) M and Re distributions

(c) C_l and L/D distributions

(d) C_T and C_P distributions

Fig. 11 Comparison of each case results along the normalized radius.

that is, the distribution of Re is decreased at each airfoil section in Fig. 11 (b). However, even though *L/D* is generally decreased according to the decrease of *Re*, the *L/D* distribution of Cases 2 and 3 increases by 34.7 % by using the airfoil shape optimization in Fig. 11 (c). The compressibility effect can be ignored because of the very low Mach number distribution in Fig. 11 (b). Case 3 results are somewhat similar with those of Case 2. However, because *D* of the blade shape in Case 3 is slightly longer than that of Case 2, the power coefficient distribution, dC_p/dx, decreases along the radial section in Fig. 11 (d).

5.5 Off-Design Analysis

Since MAVs spend most of its flight at the loiter velocity, the off-design conditions do not strongly affect the overall performance[2]. However, the off-design analysis needs to estimate the performance of the optimized propeller along the overall operating range.

Figure 12 represents the off-design analysis result for the optimized propellers of Case 3. As the flight velocity increases, the maximum propeller efficiencies increase. The increase of η_p is due to the enhancing aerodynamic performance with increasing *Re*. As the velocity decreases, maximum propeller efficiencies are achieved at a lower rpm. The maximum efficiency of the propeller of Case 3 is 81.6 % at 15.65 *m/s*.

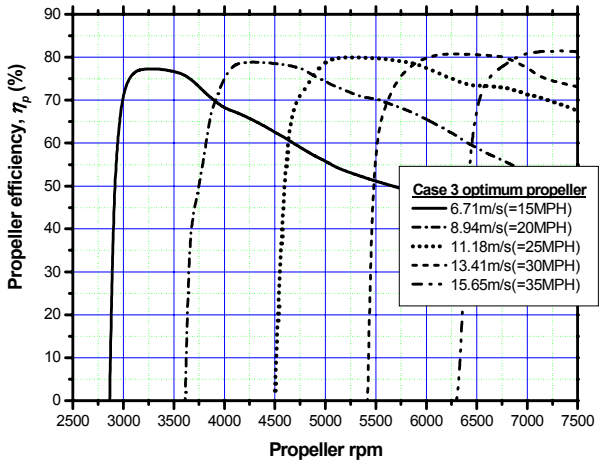

Fig. 12 Off-design analysis result of optimized propellers.

6. Conclusion

A reliable and efficient design optimization process was developed for the 3-D micro-propeller. The propeller blade shape was quickly optimized to obtain the maximum η_p according to the design requirements at the loiter velocity and altitude. To manage 143 design variables effectively, the two-step optimization procedure was established: the operating condition optimization, and the geometric design.

The initial design space for the operating condition was set up based on the performance data of Black Widow MAV. In the blade shape design optimization including the airfoil design (Case 2), *L/D* of the optimized airfoils enhanced by 34.7 % more than that in the blade shape design optimization excluding the airfoil design (Case 1). Thus, the maximum η_p of 80.9 % was achieved at the optimum point, which is the increase by 6.1 % comparing with the initial value.

To find a global optimum, design optimization was added to the probability approach (Case 3). The design space of Case 2 was moved to the higher feasible region with Chebyshev's inequality. The probability of success improved from 2.22 % in the initial design space to 16.67 % in the converged design space. The global optimal point was located at the new space outside the initial design space, and it was 1.34 *W* of *P*, 0.1016 *cm* of *D*, and 5666 of rpm at the 81.0 % of the maximum η_p. Because a reasonable initial design space was chosen, the maximum η_p of Case 3 was slightly higher than that of Case 2. Finally, the reliability of the design process was validated by comparing it with the propeller performance data of the Black Widow MAV and by analyzing the off-design conditions.

The present optimal design procedure was reliable and could be used as a practical design tool for the micro propeller development.

Acknowledgments

The study was supported by the Brain Korea-21 Program (BK21) for the Mechanical and Aerospace Engineering Research at Seoul National University and by the Center of Innovative Design Optimization Technology (iDOT), Korea Science and Engineering Foundation.

References

(1) McMichael, J. M., and Francis, M. S., "Micro Air Vehicles - Toward a New Dimension in Flight," DARPA Report, USA, Aug. 7, 1997

(2) Grasmeyer, J. M., and Keennon, M. T., "Development of the Black Widow Micro Air Vehicle," *fixed and flapping wing aerodynamics for Micro Air Vehicle Applications*, edited by Mueller, T. J., Progress in Aeronautical Sciences, Vol. 195, AIAA, 2001, pp. 519-535.

(3) Dornberger. R., Stoll. P., Büche. D., and Neu. A., "Multidisciplinary Turbomachinery Blade Design Optimization," AIAA Paper 2000-0838, January 2000.

(4) Glauert, H., *The Elements aerofoil and airscrew theory*, 2nd ed., Cambridge : Cambridge Univ. Press, 1948. pp. 199-219.

(5) Bet, A., with appendix by Prandtl, L., "Screw propellers with Minimum Energy Loss," Göttingen Reports, 1919, pp. 193-213.

(6) Larrabee, E., "Practical Design of Minimum Induced Loss Propellers," *Society of Automotive Engineers, Business Aircraft Meeting and Exposition*, Wichita, KS, April 1979.

(7) Adkins, C. N., Liebeck, R. H., "Design of Optimum Propellers," *Journal of Propulsion and Power*, Vol. 10, No. 5, September-October 1994, pp. 676-682.

(8) Lee, K. H., Jeon, Y. H., Bae, E. S., Lee, D. H., and Lee, K. T., "Implementation of the Numerical Optimization for the Micro-Air Vehicle Propeller," AIAA Paper 2004-4428, August 2004.

(9) Raymer, D. P., *Aircraft Design: A Conceptual Approach*, 3rd ed., AIAA Education Series, AIAA, Reston, 1999, Chap. 13.

(10) Roskam, J., Lan, C. E., *Airplane Aerodynamics and Performance, Design, Analysis and Research Corporation*, DARcorporation, 1997, Chap. 7, pp. 265-330.

(11) Myers, R. H., and Montgomery, D. C., *Response Surface Methodology: Process and Product Optimization Using Designed Experiments*, John Wiley & Sons, Inc., New York, 1995.

(12) Drela. M., "XFOIL: An Analysis and Design System for Low Reynolds Number Airfoil," *Low Reynolds Number Aerodynamics*, edited by Mueller, T. J., Springer-Verlag, New York, 1989, pp. 1-12.

(13) Hicks, R., Henne, P., "Wing Design by Numerical Optimization," *Journal of Aircraft*, Vol. 15, No. 7, July 1978, pp. 407-412.

(14) Vanderplaats, G. N., *Numerical Optimization, Techniques for Engineering Design: With Applications*, 3rd ed., McGraw Hill, New York, NY, 1984.

(15) Mueller, T. J., "Aerodynamic Measurement at Low Reynolds Numbers for Fixed Wing Micro Aerial Vehicles," RTO AVT/VKI Special Course on Development and Operation of UAVs for Military and Civil Applications, VKI, Rhode-Saint-Genese, Begium, Sept. 1999.

(16) Arora, J. S., *Introduction to Optimum Design*, McGraw-Hill, 1989.

(17) Mavris, D. N., Bandte, O. and DeLaurentis, D. A., "Determination of System Feasibility and Viability Employing a joint Probabilistic Formulation," AIAA Paper 99-0183, January 1999.

(18) Jeon, Y., Park, E., Kim, Y., Jun, S., Ku, Y. and Lee, D., "Feasibility Improvement of Design Space Using Probabilistic Approach," AIAA paper 2004-0537, January 2004.

(19) Grundy, T. M., and Lowson, M. V., "Effects of Acoustic Disturbance on Low Re Aerofoil Flows," *fixed and flapping wing aerodynamics for Micro Air Vehicle Applications*, edited by Mueller, T. J., Progress in Aeronautical Sciences, Vol. 195, AIAA, 2001, pp. 91-113.